



**Magnetite nanoparticles program the assembly, response,
and reconfiguration of structured emulsions**

Journal:	<i>Soft Matter</i>
Manuscript ID	SM-ART-09-2018-001931.R1
Article Type:	Paper
Date Submitted by the Author:	01-Nov-2018
Complete List of Authors:	Prileszky, Tamás; University of Delaware, Department of Chemical and Biomolecular Engineering Furst, Eric; University of Delaware, Chemical Engineering

Cite this: DOI: 10.1039/xxxxxxxxxx

Magnetite nanoparticles program the assembly, response, and reconfiguration of structured emulsions[†]

Tamás A. Prileszky^a and Eric M. Furst^{*a}Received Date
Accepted Date

DOI: 10.1039/xxxxxxxxxx

www.rsc.org/journalname

Endoskeletal droplets—non-spherical emulsion droplets that respond to external stimuli with shape change—are modified with ferromagnetic iron oxide nanoparticles to make them susceptible to magnetic fields. The resulting droplets can be manipulated with static or oscillating magnetic fields, each producing a different response. Static fields control the orientation and position of droplets, important in driving assembly into organized structures. Oscillating fields are shown to cause magnetic hyperthermia in ferrofluid nanoparticles, leading to droplet heating and forcing droplet reconfiguration. We demonstrate the use of static and dynamic fields to affect the organization and stability of endoskeletal droplets and their assemblies, producing highly-tunable programmable colloids that adapt to changing environmental conditions.

1 Introduction

Responsive soft materials adapt to the conditions of their surroundings by changing shape, mechanical, or optical properties in much the same way living cells respond to changes in their environment through taxes and tropisms. These dynamic materials draw their multiple functionalities from a library of programmable responses and include microscopic muscles^{1,2}, swimming particles^{3–5}, and reconfigurable metamaterials⁶. Enabling these responses requires dynamic colloids to be stable in multiple configurations or states and able to transition between stable states when subjected to external stimuli. For instance, the colloidal muscles studied by Shah and coworkers remain contracted until stretched by an electric field²; these assemblies have distinct configurations that external conditions toggle between. Incorporating similar responses into new colloidal materials will allow them to fill multiple roles, such as depositing to surfaces and desorbing once an active ingredient has been delivered.

Emulsions see frequent use as materials in cosmetics⁷, agrochemicals⁸, and pharmaceuticals⁹, but these are rarely designed to respond to external stimuli. Until recently, the difficulty in realizing responsive, liquid-based colloids has stemmed, in part, from their inability to maintain complex shapes: surface tension drives the liquids of emulsion droplets to relax into spheres to minimize surface area and total interfacial energy of an emulsion¹⁰. Because spherical droplets cannot occupy multiple stable shapes, their responsiveness is limited to chemical triggers^{11,12} or breakage and reformation.¹³ Typical emulsions, then, have characteristics that seem too restrictive for applications as active colloidal

materials.

Endoskeletal droplets are new materials that circumvent the shape limitations imposed by surface tension with a yield-stress network in the droplet interior^{14,15}. In these droplets, an internal network consisting of needle-shaped crystallites suspended in the liquid oil phase intercalate to form a droplet-spanning, structural framework that resists surface tension to enable non-spherical droplets without sacrificing their liquid interface or ability to solvate chemical species. The internal network is responsible for droplet responsiveness: by increasing the relative strength of interfacial tension over internal elasticity, droplets are driven to change shape to spheres¹⁶. Shape change occurs when interfacial tension is increased or when the internal network is weakened by increased temperature¹⁷. The shape-response of endoskeletal droplets extends the properties of active matter to emulsions: maintaining stability in multiple states and transitioning between states when prompted by an external stimulus.

In this study, we produce magnetically responsive endoskeletal droplets by incorporating ferromagnetic nanoparticles, making them susceptible to external magnetic fields. These droplets respond to both static and high-frequency fields. We demonstrate that static fields control the orientation and position of endoskeletal droplets, which are used to promote assembly into ordered structures. High-frequency fields induce magnetic hyperthermia of the dispersed nanoparticles^{18,19} in the droplets and elicit droplet shape change as a result. The magnetic endoskeletal droplets we produce demonstrate that engineered emulsions are indeed a class of active matter, expanding the library of responsive colloids to emulsion materials.

^a Department of Chemical and Biomolecular Engineering, University of Delaware, Newark, DE, USA. Tel: +1 (302) 831-0102; E-mail: furst@udel.edu

2 Experimental Methods

2.1 Materials

Endoskeletal droplets consist of a mixture of hexadecane and petrolatum in varying weight fractions^{14,17,20}. The petrolatum crystallizes into a yield stress network that resists surface tension acting on the liquid hexadecane interface.

In this study, we functionalize the droplets by adding a ferrofluid (Ferrotec EFH3) to the droplet mixtures. EFH3 is an oil-based ferrofluid, consisting of 10 nm magnetite particles dispersed in a mixture of C₁₁–C₁₆ branched alkanes and stabilized with a proprietary surfactant. It has a saturation magnetization of 650 gauss (G), an initial magnetic susceptibility of 3.52, and a particle mass loading of 54.4%. Petrolatum is a poor dispersant, particularly for the iron oxide nanoparticles (magnetite) in ferrofluids: adding the magnetic particle-laden ferrofluids to any solution containing petrolatum results in rapid, irreversible aggregation into large, micron-sized magnetite clusters. We use a variety of mixtures in order to observe the behavior of endoskeletal droplets with varying magnetic susceptibilities: an aggregated dispersion of strictly ferrofluid and petrolatum, a mildly aggregated mixture of petrolatum, hexadecane, ferrofluid, and a cosolvent, and a dispersed mixture prepared from the previous formulation through sedimentation of aggregates. The aggregated dispersion consists of 60% petrolatum and 40% EFH3 by weight and is characterized by large aggregates that sediment rapidly. The mildly aggregated dispersion is formulated with 15% decane, 15% hexadecane, 10% EFH3, and 60% petrolatum by weight. Here, the aggregates that form are small and remain suspended while the petrolatum fraction is crystalline. The dispersed sample is prepared by heating the mildly aggregated mixture to 80 °C to melt the petrolatum, then allowing larger aggregates to sediment overnight. The approach used to select decane as a suitable cosolvent is discussed in the supplemental materials.

The aggregated mixture has a magnetite mass fraction of 8.2%. The final mass fraction of magnetite particles in the mildly aggregated endoskeletal droplet formulation is 2.9% from thermogravimetric analysis, reduced from 5.5% prior to sedimentation. A mass balance calculation gives a final dispersed endoskeletal droplet formulation comprising: 2.9% Fe₃O₄, 4.7% EFH3 solvent, 15.4% decane, 15.4% hexadecane, and 61.6% petrolatum. A summary of all endoskeletal droplet formulations is provided in Table 1. The requirements of the experiment determine which mixture is used: under static magnetic fields, the dispersed sample has a large enough susceptibility and is used, but alternating magnetic fields require the mildly and highly aggregated dispersions because the applied field is weaker.

2.2 Droplet Production

Endoskeletal droplets are formed continuously in a microfluidic device. The process of generating these oil-in-water emulsions is discussed in detail elsewhere^{15,21}. Briefly, polydimethylsiloxane-on-glass microfluidic devices generate droplets in a T-junction heated above the 5–50 °C melting temperature of petrolatum by a Peltier device (TE Technology TE-23-1.0-1.3P). Droplets are dispersed in an aqueous surfactant solution of 10 mM sodium do-

Table 1 Three endoskeletal droplet mixtures are used experimentally with differing nanoparticle stability. In the first mixture, nanoparticles aggregate rapidly; in the second, nanoparticles aggregate slowly and to a lesser extent; the third mixture contains no visible aggregates. For each mixture, the weight fractions of petrolatum, hexadecane, decane, magnetite, and EFH3 ferrofluid solvent are listed.

Sample	w_{Pet}	w_{Hex}	w_{Dec}	w_{Mag}	w_{EFH3}
Aggregated	0.704	—	—	0.082	0.214
Mildly aggregated	0.600	0.150	0.150	0.055	0.046
Dispersed	0.616	0.154	0.154	0.029	0.047

decyl sulfate (SDS) above the critical micelle concentration. Syringe pumps are used to vary the relative flow rates of the aqueous (continuous) and endoskeletal droplet (dispersed) streams and control droplet size and frequency, where greater dispersed-to-continuous-phase flow rate ratios $\frac{Q_D}{Q_C}$ correspond to larger droplets²². The melted endoskeletal droplet precursors flow away from the T-junction and towards decreasing temperatures, allowing the petrolatum to crystallize and form the yield-stress internal network unique to endoskeletal droplets. The microfluidic channel walls mold endoskeletal droplets into non-spherical shapes. Once crystallized, droplets are ejected from the microfluidic device into a reservoir where coalescence between droplets can be promoted or prevented by decreasing or increasing droplet crystallinity, respectively. Droplet crystallinity at the device outlet is dictated by residence time in the channel: increasing residence time increases the crystallinity of droplets upon ejection¹⁵. Coalescence is eliminated at any crystallinity by preventing collisions between droplets.

2.3 Magnetic Manipulation

We investigate two modes of manipulating magnetically-functionalized endoskeletal droplets: by applying steady magnetic fields using permanent magnets or through the use of alternating fields generated by an electromagnetic coil. The permanent magnets are neodymium (K&J Magnetics, D72-N52) and are placed between 0.5 and 2 cm from the microfluidic outlet, yielding a magnetic field strength from 50–500 G.

An alternating magnetic field is generated by an induction heating circuit adapted from RM Cybernetics consisting of a zero-voltage resonant switch²³. The LC circuit of the oscillator comprises a 12-turn, 62-stranded Litz wire coil in parallel with a 0.4 μF bank of capacitors. The circuit oscillates at 1.08 MHz and is supplied a current of 4.6 A from a DC power supply. The resonant frequency of an LC circuit is $f_0 = \frac{1}{2\pi\sqrt{LC}}$, where f is frequency in hertz, L is inductance in henries, and C is capacitance in farads; this equation yields an induction coil inductance value of 54 nH. At experimental conditions, the coil generates fields in excess of 20 G before electrical resistance causes passive heating of the sample; to eliminate the effect of passive heating, the coil is isolated in a box and air-cooled with compressed air. The inside of the coil is sheathed in plastic, preventing either the coil or cooling air from directly touching the sample. The temperature change associated with induction heating is measured in 1 mL samples of ferrofluid mixtures added to 1.5 mL centrifuge tubes placed in the

induction coil. Temperatures are recorded every second with an infrared thermometer.

3 Results

3.1 Static magnetic fields

The actions of a responsive colloid can be localized to target environments by using directing fields to control their motion. Static magnetic fields can be used to impose a motive force on magnetic materials, enabling precise manipulation of the position of a magnetic particle by modulating field strength and location. Moreover, magnetic fields have an intrinsic orientation, which permits control of particle rotation. Both properties are useful for controlling endoskeletal droplet response.

Applying a static magnetic field near the outlet of a microfluidic device that is producing magnetically-functionalized droplets has several useful applications. First, droplets produced in the absence of a field float to the surface of the reservoir they are ejected into due to their buoyancy, as depicted in Figure 1a. Over time, droplets crowd over the ejection point of the device, creaming into a heterogeneous film with poorly-defined droplet shapes. Applying a directing field near the device outlet allows droplets to be separated to an extent dependent on field strength: stronger fields separate droplets more than weaker fields, seen as the field strength is increased between Figure 1b and 1c by moving the magnet closer to the device outlet. Droplets also reorient in the direction of the applied field. However, because the droplets are in motion, the contribution of the field to their orientation is combined with reorientation due to hydrodynamic resistance and interactions.

When the same field is applied to droplets that are coalesced into chains, similar responses are observed: chains deflect in the direction of the applied field, and individual droplets in the chain assume the field orientation, shown by the contrast between field-off and field-on states in Figure 1d and 1e, respectively. Droplet chains deflect to a greater extent than free droplets because of the cascading pull of the magnetic field on each subsequent link in the chain, a characteristic that is also responsible for the rotation of droplets in this case. As the droplets in the chain proceed along the field gradient toward increasing field strength, they experience a larger magnetic moment. The physical linkages between droplets—their coalesced necks—create a medium through which the magnetic moment can be transmitted down the chain, increasing deflection out of the device over isolated droplets. In addition, the strong tendency to orient along the field gradient suggests that, by toggling between static fields generated at the top and bottom of the reservoir, it is possible to overcome the natural periodicity of chain folding apparent in Figure 1d.

The non-spherical shapes of endoskeletal droplets make orientation as important to control as their position because it affects the adsorption, flow properties, and surface coverage of droplets. Correspondingly, it is valuable to separate the effects of an applied magnetic field and motion-induced drag on the reorientation of droplets. Figure 2 contains images of droplets under fields applied from different directions.

In Figure 2a, no external field is, or has been, applied, so the

droplets are oriented randomly. When a field is applied to the top of the image as in Figure 2b, droplets move slightly toward the field source and reorient in the field direction; importantly, droplets rotate prior to translating, visible in the supplementary video clip of Figure 2. In Figure 2c, a weaker field is applied to the bottom of the image, causing droplets to reorient without significant translation.

Magnetically-polarized endoskeletal droplets begin to interact at higher densities, allowing organized superstructures to be built. In Figure 3, applying a magnetic field in a sufficiently dense suspension of magnetic droplets leads to chaining. In the first frame, droplets have been concentrated using a magnetic field, but are still disoriented because the field was applied perpendicular to the imaging plane. When the field is directed parallel to the imaging plane and to the left of the image, droplets align in the applied field direction, as in Figure 2, but the droplets are close enough together to interact and chain. Chaining is more apparent in the third frame, where long droplet structures begin to emerge. This behavior is analogous to the chaining of smaller magnetic particles in external magnetic fields²⁴.

Droplet superstructures also have preferred modes of shape reconfiguration. Regions between adjacent droplets have a high interfacial curvature, which makes them more susceptible to coalescence and reconfiguration than the flat faces.²⁵ As a result, as a droplet assembly is heated, individual droplets melt and coalesce, which is followed by folding along boundaries between droplets. This folding, visible in Figure 4 is a multi-tiered response that allows droplet structures to potentially fulfill multiple roles. For instance, the droplet structure in the left-most image of Figure 4 has the largest surface area and, correspondingly, greatest propensity for substrate adsorption, while the third image has a surface area that is approximately halved. This surface area reduction limits the rate of mass transfer to the substrate while still maintaining a low projected area from the surface and high contact area, preventing desorption. When collapse is driven to completion, or the formation of a spherical droplet in the right-most image, the projected area is increased and the surface area in contact with the substrate is reduced, which promotes removal from the surface. Droplets with these characteristics make interesting delivery vehicles because they allow control over both the rate of active ingredient delivery and adhesion to the target site, enabling delivery rate to be tuned or stopped altogether as the application requires.

In linear droplet structures, complex folding is also observed, meaning that even simple droplet assemblies can occupy several states. In the simplest case of a droplet doublet, as in Figure 5a, three discrete geometries are observed. First, the aligned linear doublet itself, with a large surface area and low thickness. Second, once droplet collapse is triggered—either by heating or contact with a foreign object such as a fiber or particle—the doublet folds in half. Finally, the droplet doublet is heated to remove its internal structure, allowing complete collapse to a sphere. The droplet folds away from the glass surface it is adsorbed to, reducing contact area as reconfiguration proceeds, which is shown in a rendered droplet structure for clarity in Figure 5. In addition to affecting the adsorption of droplets to substrates, this shape

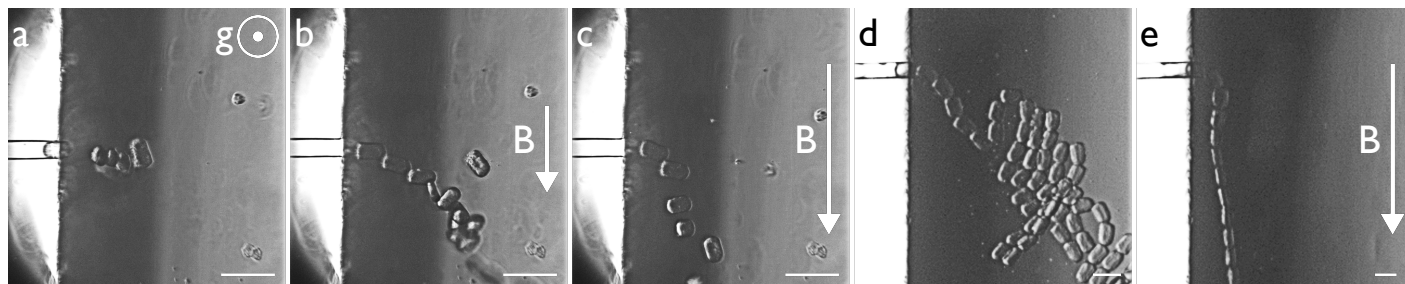


Fig. 1 Response of droplets and assemblies to a static magnetic field at the outlet of a device: (a) is magnetic droplets in the absence of a field driven into the page by buoyancy, (b) depicts the same droplets under a moderate applied field, while (c) is a stronger field. In (d), droplets are coalesced into chains without a field, and in (e), the same droplet chains are deflected with a static field. When present, arrows indicate the direction and qualitative magnitude of the applied field. Scale bars are 100 μm .

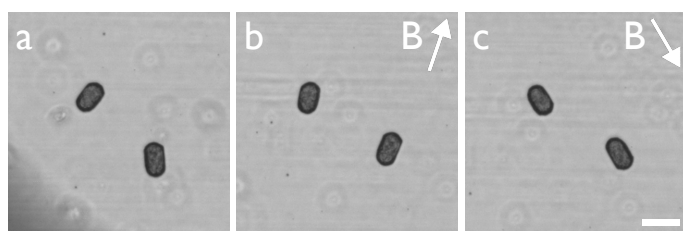


Fig. 2 Droplets reoriented by an applied static magnetic field. Droplets have a shape-induced magnetic dipole; the magnetic field gradient favors droplet orientations with the long axis parallel to the magnetic field lines. As a result, droplets can be reoriented while negligibly affecting position. Arrows indicate the direction of the applied magnetic field. Scale bar is 100 μm .

response may be used to trap material on a substrate to aid in separation and purification.

When droplet structures are extended, it is unlikely that reconfiguration occurs at the center of the assembly. Instead, folding occurs nearer the ends where there is less contact for the chain to desorb and start folding. As a result, folding leads to rolling, illustrated in Figure 5b. The weakening of the internal network and local high curvature cause the droplet at the far right of the structure to fold inward. The liquid meniscus that forms between the folded droplet and the remainder of the chain continues “pulling” the rolled section down the chain, leading to a continuous collapse until the original chain forms an oblong droplet.²⁶ The shape change completes when the droplet forms a sphere, which is accomplished by additional heating. An interesting outcome of this mechanism of collapse is that it allows new droplet shapes to be formed; for instance, long chains continue folding inward, eventually forming a discoid droplet.

3.2 Magnetic hyperthermia

Static magnetic fields are powerful tools for manipulating magnetically-functionalized endoskeletal droplets, particularly for controlling orientation, position, and assembly. However, they do not provide a route to enable droplet response; for this, high-frequency, alternating magnetic fields can be used. High-frequency fields induce significant heating in both bulk materials—commonly referred to as induction heating—and in dispersions of magnetic nanoparticles. Such ‘magnetic hyper-

thermia’ has been demonstrated in a variety of nanoparticle dispersions^{18,19}. The benefits of magnetic nanoparticle heating are most apparent when used for targeting: nanoparticles or nanoparticle carriers can be concentrated at a target site using a static magnetic field, then heated with a high frequency field, only affecting their immediate surroundings. In endoskeletal droplets, this property is capable of eliciting shape reconfiguration.

Heating the endoskeletal droplets using induction has properties distinct from bulk heating of an emulsion system. Of particular interest is the potential for targeted droplet response: only droplets exposed to the magnetic fields are heated, causing localized shape change. Because the energy transmitted to the nanoparticles is dissipated primarily in the droplets, the surrounding continuous phase of the emulsion does not change temperature, which is useful in delivery applications where indiscriminate heating of the system as a whole is undesirable or harmful, such as in sensitive body tissues. In addition, heating through induction is less limited by heat transfer than bulk heating: droplets are small and have a near uniform distribution of particles, so heat transfer length scales are negligible—on the order of 100 nm for droplets of the dispersed mixture—meaning droplets are approximately at the temperature of the nanoparticles throughout heating. An induction heater capable of delivering more power to the dispersions than the experimental apparatus would thus cause rapid restructuring of droplets, limited only by the rate of nanoparticle heating.

The primary benefit of induction-heating endoskeletal droplets is that it provides a route to remotely change droplet shape without affecting the surrounding medium. The internal network of the droplets is stronger than surface tension, but the balance of forces can be overcome by either increasing surface tension or lowering the network yield stress; the former can be accomplished by reducing surfactant concentration, whereas the latter is most easily accomplished by increasing temperature to melt the network. Although the changes in temperature associated with induction heating in endoskeletal droplet mixtures are low—3 and 5.5 $^{\circ}\text{C}$ for 2.9 and 5.4% particle loadings, respectively—the moderate temperature changes are sufficient to soften the petrotatum internal network and induce droplet relaxation. Figure 6 demonstrates the collapse of a random network of endoskeletal droplet chains at 5.4% particle loading under induction heating.

The weakening of the internal network due to melting of petro-

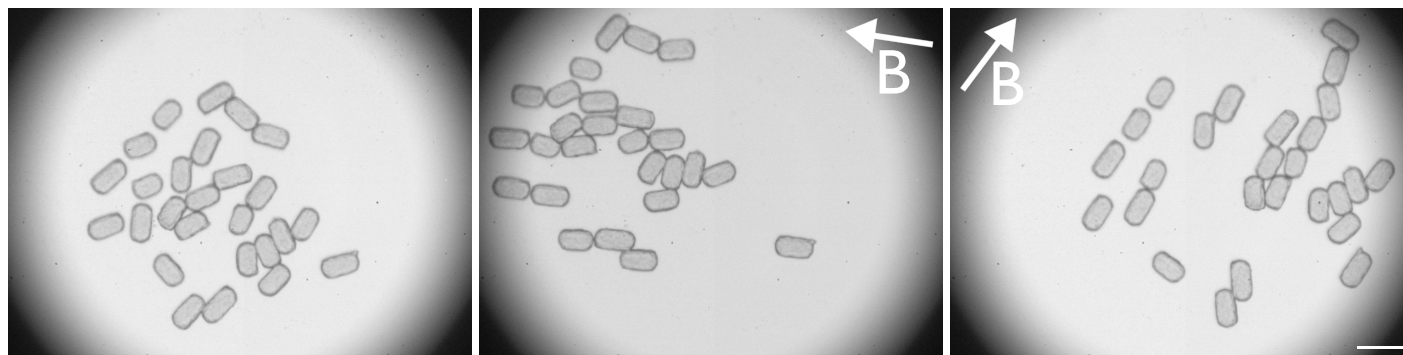


Fig. 3 Dense array of magnetic endoskeletal droplets exposed to a static magnetic field. When present, arrows indicate the direction of the applied magnetic field. Droplets reorient from a concentrated but disorganized state, aligning in the direction of the applied field to form a nematic arrangement of droplets. When the field is moved to the top of the image, droplets reorient again, breaking the previous structure and forming elongated droplet structures in the direction of the new field. Scale bar is 100 μm .

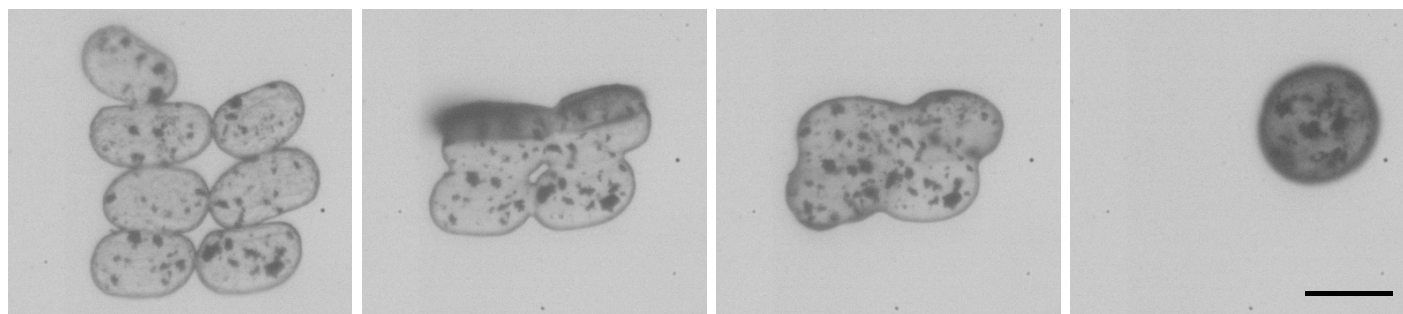


Fig. 4 Droplets concentrated and aligned in an magnetic field are heated to collapse. Here, the field is not present, but the structure it induced persists. While heating, the droplets sinter to form a flat droplet mat with regions of high and low curvature—joints between droplets maintain a higher curvature than the flat tops of droplets. As heating continues, the regions of high curvature fail, causing the mat to fold and doubling its thickness while halving its surface area. Scale bar is 100 μm .

latum crystallites reduces the interfacial curvature that the internal crystallite network can support, so the droplet chains coarsen until the yield stress of the internal network and surface tension balance. The transformation of Figure 6 does not proceed to completion—the formation of spheres—because the network is not completely melted. This demonstrates that the collapse of endoskeletal droplets can be arrested at any point by removing the alternating field, which allows the internal network to cool and reform, preserving the shape produced by the collapse process. By causing selective transformation of the droplet network, it is possible to develop materials that undergo a staged response, allowing tiered delivery of an active ingredient or selective delivery in polydisperse emulsions, where some droplets are less stable against collapse. Applying an external field through a small wire or coil would localize heating further, allowing individual droplets to be melted and driving local response of a droplet assembly or ‘welding’ droplets together.

4 Discussion

A number of parameters affect the assembly and response of magnetically-functionalized endoskeletal droplets, including droplet composition ϕ_p , surface tension γ , aqueous phase viscosity μ_a , droplet size and shape, magnetite mass fraction ϕ_m , and temperature. In this section, we consider the physical forces and their magnitudes governing magnetic droplets in an effort to un-

derstand our experiments and to provide a rational parameter design space for engineering their responsiveness and reconfigurability. Specifically, the induced magnetic forces and interactions and hydrodynamic drag dictate their translation, rotation, interactions, and corresponding characteristic timescales.

In Figure 7, we summarize the three modes of response described in the results section that a droplet undergoes when exposed to an external magnetic field generated by a static magnet: translation towards the field source, rotation to align with the field, and assembly through translation towards neighboring droplets. Each relies on a different aspect of the magnetic field. The torque depends on the magnitude of the field and induced moment of the droplet; translation is governed by the magnitude and gradient of the applied field and the induced moment; and assembly arises from the interaction of the induced moments. While these responses are coupled, the field can be manipulated to favor one mode over another, as our experimental results have shown.

4.1 Magnetic interactions

The interactions between droplets and the external field are governed by the shape-induced magnetic moment, which we approximate by

$$\mathbf{m}_d = V_d \left[\frac{\chi_d \mathbf{B}}{1 + 4\pi\chi_d n} \right] \quad (1)$$

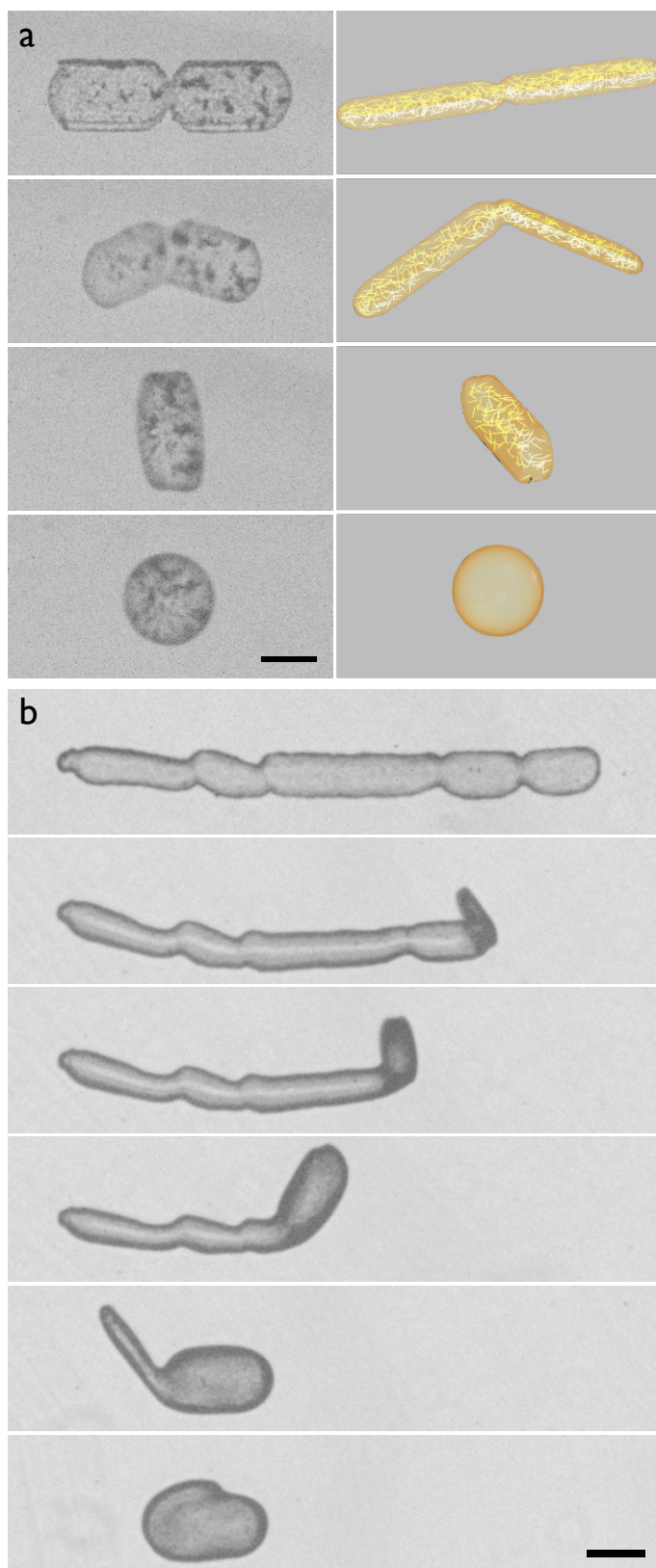


Fig. 5 In a, a droplet doublet is driven to collapse. A 3D render of a folding droplet is shown at the right for clarity: the two droplet lobes fold together to reduce surface area, forming a second shape with approximately half the surface area and twice the thickness. The collapse is then driven further, which produces a spherical droplet. Scale bar is $50\ \mu\text{m}$. In b, a slightly curved droplet chain is heated, causing the droplets “roll” inwards. The rolling continues to the end of the chain, and an oblong droplet remains. Scale bar is $100\ \mu\text{m}$.

Table 2 Summary of endoskeletal droplet mixture magnetic properties. Torques are calculated for a droplet perpendicular to the field direction. Interaction energies are calculated at a separation of $100\ \mu\text{m}$.

Sample	χ_d (—)	\mathbf{m} ($\text{A m}^2 \times 10^{12}$)	τ ($\text{N m} \times 10^{15}$)	E_{mm} ($\text{J} \times 10^{17}$)
Aggregated	0.44	8.8	2.8	15
Mildly aggregated	0.34	6.9	2.2	9.4
Dispersed	0.27	5.5	1.7	6.0

for a general ellipsoidal droplet.²⁴ Here, V_d is the droplet volume, χ_d is the magnetic susceptibility of the droplet fluid, and n is the demagnetizing factor, which is a function of the droplet shape, defined as

$$n = \frac{R_1 \cdot R_2 \cdot R_3}{(R_1^2 - R_2^2)(R_1^2 - R_3^2)^{\frac{1}{2}}} [F(k, \phi) - E(k, \phi)]. \quad (2)$$

As aspect ratio increases, n decreases with a corresponding increase in magnetic moment.

The magnetic field is generated by a neodymium magnet, which can be treated as a separate dipole, especially at large separations. The magnetic field strength was measured at varying distances from the magnet to estimate the magnetic moment assuming $\mathbf{m}_m = \mathbf{M}V_m$, where \mathbf{M} is the uniform magnetization of the magnet and V_m is the magnet volume. The magnet used experimentally has a magnetization of $\sim 30\ \text{kA m}^{-1}$; this value is used to estimate the magnetic field strength according to

$$H_{\text{mag}} = \frac{2\mathbf{m}_m}{4\pi r_m^3} \quad (3)$$

or the dipole-dipole interaction energy using

$$E_{\text{DD}} = \frac{\mu_0 \mathbf{m}_d \mathbf{m}_m}{2\pi r_m^3}. \quad (4)$$

In both Equation 3 and 4, r_m is the distance from the magnet and the quantities are calculated along the axis of magnetization for aligned dipoles.

The experimental droplet shape is approximated as a triaxial ellipsoid with radii $R_1 = 50$, $R_2 = 20$, and $R_3 = 12.5\ \mu\text{m}$. Droplets of different magnetite loading have different magnetic susceptibilities; using the respective value for each formulation yields the magnetic moment, maximum torque, and dipole interaction energies droplet experience, summarized in Table 2 for a magnetic field strength of $250\ \text{A m}^{-1}$. Magnetic susceptibilities are estimated based on Bruggeman’s model of a medium with spherical inclusions.²⁴ Increasing magnetic particle loading leads to larger magnetic moments, higher orienting torques, and stronger dipole-dipole interaction energies, but the absolute magnitudes of these quantities does not determine their relative rates.

4.2 Hydrodynamic forces

We also consider the fluid forces counteracting the droplet motion to determine the rate at which a specific mode of transport will occur. For a general, triaxial ellipsoid, the hydrodynamics of drag are approximated by Perrin.²⁷ Using the same ellipsoidal dimensions as used to calculate the droplet magnetic moment, the

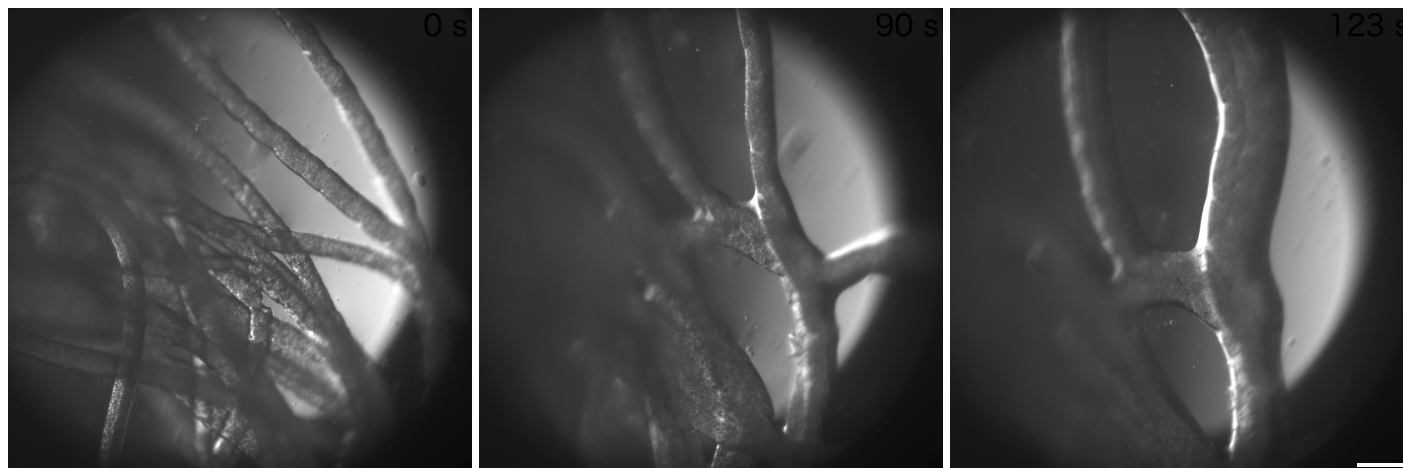


Fig. 6 Collapse of a droplet network as the result of induction heating. The fluid network comprises the endoskeletal droplet mixture at 5.4% particle loading. Scale bar is 100 μm .

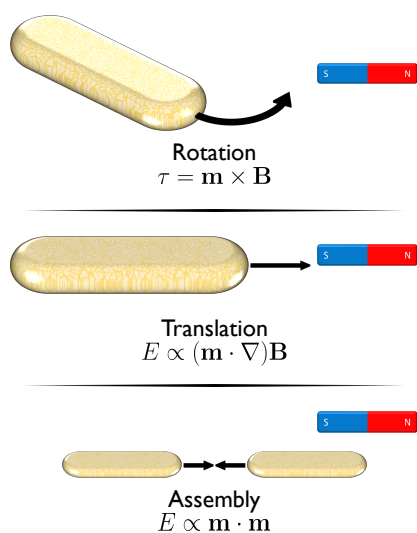


Fig. 7 Three modes of droplet transport mediated by external magnetic fields: rotation in registry with the external field direction, translation towards the magnetic field source, and assembly by translation towards other magnetic droplets.

rotational friction factors C about axis i are defined as

$$C_1 = \frac{16\pi\eta}{3} \frac{R_2^2 + R_3^2}{R_2^2 P_2 + R_3^2 P_3} \quad (5)$$

$$C_2 = \frac{16\pi\eta}{3} \frac{R_1^2 + R_3^2}{R_1^2 P_1 + R_3^2 P_3} \quad (6)$$

$$C_3 = \frac{16\pi\eta}{3} \frac{R_1^2 + R_2^2}{R_1^2 P_1 + R_2^2 P_2} \quad (7)$$

where η is the viscosity of the medium and R_i is the dimension of semiaxis i . The translational friction factor in the direction of axis i is

$$f_i = \frac{16\pi\eta}{S + R_i^2 P_i} \quad (8)$$

In Equations 5–8, P and S are the elliptic integrals

$$P_i = \int_0^\infty \frac{ds}{(R_i^2 + s) \sqrt{(R_1^2 + s)(R_2^2 + s)(R_3^2 + s)}} \quad (9)$$

$$S = \int_0^\infty \frac{ds}{\sqrt{(R_1^2 + s)(R_2^2 + s)(R_3^2 + s)}} \quad (10)$$

that satisfy

$$P_1 + P_2 + P_3 = \frac{2}{R_1 R_2 R_3} \quad (11)$$

$$S = R_1^2 P_1 + R_2^2 P_2 + R_3^2 P_3. \quad (12)$$

4.3 Droplet mobility

The relationship between the force acting to move a droplet and that to stop it produces some mobility. From this, we define a rotational mobility $b_{\theta,i}$ about the axis i as

$$b_{\theta,i} = \frac{\tau_i}{C_i}, \quad (13)$$

or the ratio of the magnetic torque and the hydrodynamic drag. Similarly, the translational mobility along axis i is defined as

$$b_i = \frac{E_{DD}}{f_i}, \quad (14)$$

the ratio of the dipole-dipole interaction energy and the translational drag. The dipole-dipole interaction energy is calculated for a droplet and the external magnet in the case of translation or two droplets in the case of assembly.

Ratios of droplet mobilities give information about their relative rates. Two ratios are of interest; the first is that of the rotational and translational motion of the droplets. Each mobility must be scaled by a characteristic value, yielding

$$\frac{b_1 \theta_c^2}{b_{\theta,1} L_c^2}, \quad (15)$$

where θ_c is the characteristic rotation angle of $\frac{\pi}{2}$ radians and L_c is the characteristic translation length scale of one droplet length or $2R_1$. Large values of this ratio correspond to fast translation. The component ratios $\frac{b_1}{L_c^2}$ and $\frac{b_{\theta,1}}{\theta_c^2}$ both result in a characteristic time scale for transport. Under typical experimental conditions, the characteristic relaxation time $t_{\text{rot},c} \approx \mathcal{O}(10^{-1}-10^1)$ s for rotation; for translation, it is $t_{\text{trans},c} \approx \mathcal{O}(10^{-2}-10^2)$ s.

The second quantity of interest is the non-dimensionalized assembly ratio

$$\frac{b_1 t_c}{L_c^2}, \quad (16)$$

where t_c is a characteristic transport time, which is the time over which the external field is applied. Here, b_1 is the translational mobility as induced by a neighboring droplet dipole rather than the external field, and the characteristic length scale is the separation between the droplets. Correspondingly, large values of this quantity denote fast assembly. The transport and assembly ratios are calculated and plotted in Figure 8.

These dimensionless ratios reveal important features of droplet transport and assembly. First, the ratio of rotational and translational mobility is a strong function of magnetic field strength because magnetic field strength increases as $\frac{r_m}{R_1}$ decreases. At large field strengths, droplets translate readily whereas they rotate more freely at lower field strengths; above $\frac{r_m}{R_1} \approx 150$, the ratio is smaller than unity, indicating that translation is dominant. Correspondingly, the orientations of droplet assemblies can be controlled in the presence of weak field more precisely than in strong fields. In addition, at small separations between droplets $\frac{r_s}{R_1}$, assembly is fast and occurs in about 10 characteristic time spans, which agrees with experimental results from Figure 3. At larger separations, droplets take orders of magnitude longer to assemble, essentially never converging due to translation towards the external magnet.

The calculated dimensionless quantities are also predictive of the droplet relaxations observed during experiments. Two rotational transitions from Figure 2 are analyzed in Figure 8. The first is translation-dominant, with relaxation times of $t_{\text{rot},c} = 0.7$ s and $t_{\text{trans},c} = 0.6$ s, corresponding to a transport ratio of 1.03. Rotation dominates the second transition with a transport ratio of

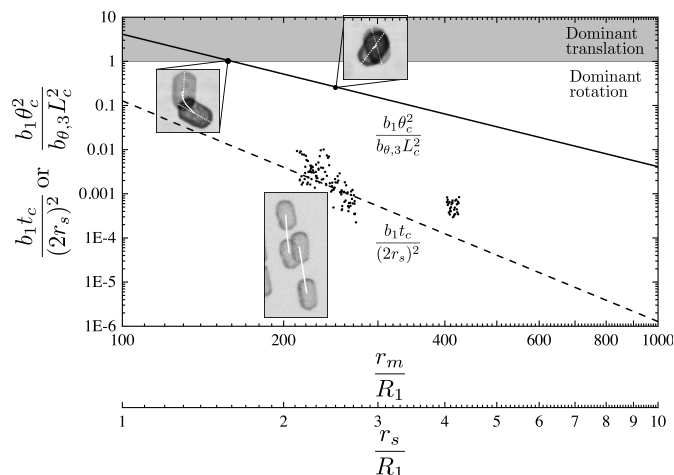


Fig. 8 Relationship between the two dimensionless quantities and a dimensionless separation. The transport ratio is calculated for translation along the major axis and rotation around the shorter minor axis and the separation is the distance between the external magnet and the droplet normalized by the droplet major axis length $\frac{r_m}{R_1}$. The inset figures at transport ratios of ~ 1 and ~ 0.25 are overlays of initial and final droplet positions with orientations represented by dotted lines and the translation trajectory depicted in solid white. For the assembly ratio, the translational mobility is calculated along the major axis of the ellipsoid and the separation is normalized by the length of the droplet major axis $\frac{r_s}{R_1}$. The inset figure next to the data points is an overlay of the trajectories of two droplets that are assembling. The individual paths are traced at the droplet centroid in white. At separations smaller than $0.1R_1$, droplets are attracted to each other strongly enough to align and chain. The ratio of rotational to translational mobility tends toward dominant rotation at large magnet separations.

0.27, coming from relaxation times of $t_{\text{rot},c} = 3.4$ s and $t_{\text{trans},c} = 12.5$ s. While the magnet separation was not measured and the applied field strength cannot be determined, the increase in transition times between translation- and rotation-dominant motion indicates that weaker fields lead to relatively faster rotation. Assembly experiments are also represented qualitatively by the dimensionless quantities. The data points in Figure 8 represent the closure rates of several droplet pairs measured as a function of interdroplet separation. The predicted values of $\frac{b_1 t_c}{(2r_s)^2}$ are closely matched by those measured experimentally from videos analogous to Figure 3. The calculations were performed assuming constant field strength at an intermediate experimental value of 250 A m^{-1} . In addition, calculated droplet assembly rates at large separations are estimates because of the field-strength gradient; the field is not uniform, so the droplet closer to the external field has a larger mobility than the farther droplet, preventing assembly. As a result, we were unable to measure assembly at larger droplet separations with our experimental setup.

4.4 High-frequency magnetic fields

As shown in the previous section, the timescales of droplet motion are slow, and therefore they do not rotate or translate in a sufficiently high-frequency field. Instead, the droplets heat. The mechanism of heating depends on the size of the dispersed magnetic material. Macroscopic conductors in alternating magnetic fields dissipate energy through electrical resistance from

the formation of eddy currents in their outermost layers due to the skin effect¹⁸. Additionally, if the conductor is ferromagnetic, the shifting of magnetic domains as they align with the applied external field causes heating through frictional dissipation. For nanoparticles, however, different mechanisms dominate because eddy currents cannot form in the small volume and nanoparticles consist of only single or a few magnetic domains. Instead, Brownian and Néel relaxations lead to heating. In the Brownian limit, an entire magnetic particle rotates to align its magnetic moment with the applied field, releasing heat through frictional losses between the particle and surrounding fluid. In Néel relaxation, the atoms that constitute the magnetic domains of a particle realign with the magnetic field rather than the entire particle rotating, causing heating through friction between atoms. Dominance of one mechanism over the other depends on several factors, but can be differentiated by their relaxation times. The Brownian relaxation time, $\tau_B = \frac{4\pi r_H^3 \eta}{k_B T}$, accounts for the particle hydrodynamic radius r_H , fluid viscosity η , and surrounding temperature T ²⁸. The Néel relaxation time, $\tau_N = \tau_0 \frac{KV_C}{k_B T}$, incorporates the attempt time τ_0 , anisotropy constant K , and particle core volume V_C ²⁹. The magnetite particles dispersed in the endoskeletal droplets—with a radius of approximately 5 nm, attempt time of 2×10^{-10} s, and an anisotropy constant of $-1.1 \times 10^{-4} \text{ J m}^{-3}$ —have Néel relaxation times $\tau_N \approx 1$ ns and Brownian relaxation times $\tau_B \approx 1 \mu\text{s}$. The significantly lower Néel relaxation time means that this is the dominant mechanism for the endoskeletal droplet system; correspondingly, higher frequency magnetic fields heat the nanoparticle dispersions more efficiently, especially as the alternation frequency approaches the Néel frequency, approximately 1 GHz for this system.

Nanoparticles, whether with single or multiple magnetic domains, experience significant heating when exposed to alternating magnetic fields with frequencies higher than approximately 500 kHz¹⁸. The experimental induction coil used to induce magnetic hyperthermia oscillates at a frequency of 1.08 MHz, well within the required frequency range to heat ferrofluid mixtures. The bulk heating of both endoskeletal droplet and EFH3 ferrofluid mixtures are tested in the induction coil, and the results are plotted in Figure 9. The temperature profiles of each formulation vary significantly, which is indicative of several features of each mixture. First, increasing magnetite mass fraction increases the final temperature because more particles are present dissipating frictional heat, and this behavior is observed in both endoskeletal droplet and ferrofluid mixtures. Second, the slopes of the ferrofluid and endoskeletal droplet temperature profiles differ greatly, with the ferrofluids heating significantly faster at the same mass fraction of magnetite. In addition, the ferrofluid mixtures reach a higher final temperature than do the endoskeletal droplet mixtures. These differences are largely the result of two aspects of the endoskeletal droplet mixtures: their crystallinity and the partial aggregation of the dispersed nanoparticles.

The heat of fusion of the crystalline internal phase in the endoskeletal droplet mixtures presents an additional obstacle to heating. As a result, dissipating the same energy in endoskeletal droplets and in ferrofluids results in a smaller temperature

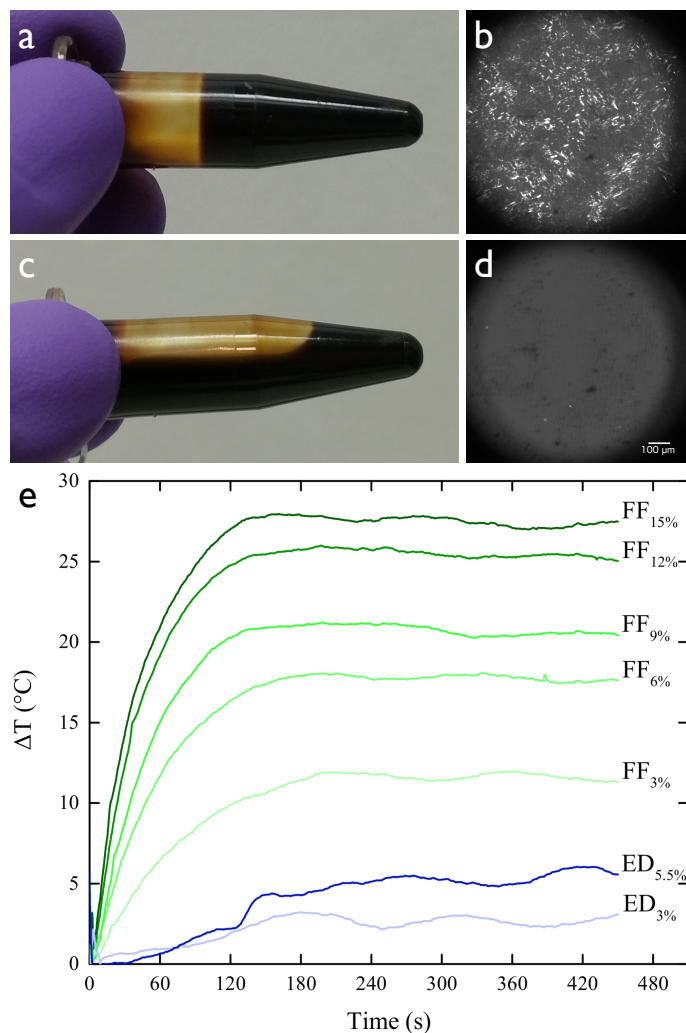


Fig. 9 Induction heating of ferrofluid mixtures. a and c demonstrate that the internal network melts upon induction heating, allowing the mixture to flow. In b and d, the melting phenomenon is shown in optical micrographs under crossed polarizers, where b is prior to heating and d is after melting. The temperature of particle dispersions is provided in e as a function of induction heating time. FF indicates ferrofluid mixtures without petroleum and ED indicates endoskeletal droplet mixtures. The mass fraction of magnetic particles in the droplets is provided in the label subscripts. The endoskeletal droplet mixture at 5.4 % particles is the mixture prior to separating aggregates. A sample without magnetite was tested, and is excluded from this figure; it would be located at zero.

change because some of the energy must be used to melt the crystalline phase. While the heat of fusion explains the difference in initial slope between the formulations, it does not explain the differing final temperatures; because the thermal diffusivities of the mixtures are nearly identical, applying the same heating stimulus should culminate in complementary temperature changes. The existence of a large discrepancy, then, must be the result of changes in heating efficiency. In the endoskeletal droplet mixtures, much of the particle aggregation is mitigated by adding decane, which is discussed in the supplementary information. However, it is not completely eliminated and the nanoparticles dispersed in endoskeletal droplets are expected to be larger than those in the ferrofluid mixtures, reducing the induction heating efficiency and explaining the difference in final temperatures reached by the ferrofluid and endoskeletal droplet mixtures.

5 Conclusions

Endoskeletal droplets are interesting materials because they introduce shape anisotropy to emulsion systems; as a result, the droplets demonstrate a variety of active behaviors such as tunable partial coalescence and responsive shape change. In this investigation, we functionalize endoskeletal droplets with magnetic nanoparticles to enhance existing droplet functions as well as introduce new ones. The resulting paramagnetic droplets respond to external magnetic fields, where the ultimate response depends both on the nature of the applied field and the state of the droplet.

Introducing magnetic materials to endoskeletal droplets expands their usefulness beyond what is possible with non-functionalized droplets and allows new applications that were previously inaccessible. For instance, endoskeletal droplets or droplet networks may be introduced as a delivery vehicle that can be deactivated—or have the rate of active ingredient delivery strongly reduced—by applying a high-frequency alternating field and causing droplets to melt. Any number of delivery vehicles could be augmented or replaced by functionalized endoskeletal droplets to improve targeting and delivery efficiency. These materials are exciting additions to the array of responsive colloids currently being researched, and they lay the groundwork for future research into active emulsion systems.

Conflicts of interest

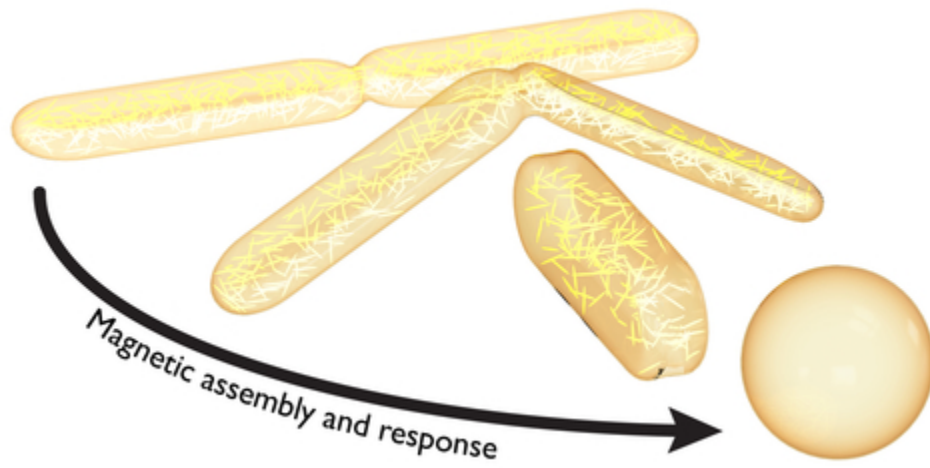
There are no conflicts to declare.

Acknowledgements

The authors would like to thank Patrick Spicer for fruitful discussions. This work was supported by National Science Foundation Grant CBET-1336132.

Notes and references

- 1 J. E. Marshall, S. Gallagher, E. M. Terentjev and S. K. Smoukov, *J. Am. Chem. Soc.*, 2014, **136**, 474–479.
- 2 A. A. Shah, B. Schultz, W. Zhang, S. C. Glotzer and M. J. Solomon, *Nat. Mater.*, 2014, **14**, 117–124.
- 3 R. Dreyfus, J. Baudry, M. L. Roper, M. Fermigier, H. A. Stone and J. Bibette, *Nature*, 2005, **437**, 862–865.
- 4 Y. Hong, N. M. K. Blackman, N. D. Kopp, A. Sen and D. Velezol, *Phys. Rev. Lett.*, 2007, **99**, 178103.
- 5 R. Soto and R. Golestanian, *Phys. Rev. E*, 2015, **91**, 052304.
- 6 J. Y. Ou, E. Plum, L. Jiang and N. I. Zheludev, *Nano Lett.*, 2011, **11**, 2142–2144.
- 7 L. Gilbert, C. Picard, G. Savary and M. Grisel, *Colloids Surfaces A Physicochem. Eng. Asp.*, 2013, **421**, 150–163.
- 8 G. M. S. ElShafei, M. M. El-Said, H. A. E. Attia and T. G. M. Mohammed, *Ind. Crops Prod.*, 2010, **31**, 99–106.
- 9 L. M. Verissimo, L. F. Agnez Lima, L. C. Monte Egito, A. G. de Oliveira and E. S. T. do Egito, *J. Drug Target.*, 2010, **18**, 333–342.
- 10 I. W. Hamley, *Introduction to Soft Matter: Synthetic and Biological Self-Assembling Materials*, John Wiley & Sons, Ltd, Chichester, UK, Revised edn, 2007, pp. 1–328.
- 11 A. San Miguel, J. Scrimgeour, J. E. Curtis and S. H. Behrens, *Soft Matter*, 2010, **6**, 3163.
- 12 O. J. Cayre, J. Hitchcock, M. S. Manga, S. Fincham, A. Simoes, R. A. Williams and S. Biggs, *Soft Matter*, 2012, **8**, 4717–4724.
- 13 S. Melle, M. Lask and G. G. Fuller, *Langmuir*, 2005, **21**, 2158–2162.
- 14 M. Caggioni, A. V. Bayles, J. Lenis, E. M. Furst and P. T. Spicer, *Soft Matter*, 2014, **10**, 7647–7652.
- 15 T. A. Prileszky and E. M. Furst, *Langmuir*, 2016, **32**, 5141–5146.
- 16 A. B. Pawar, M. Caggioni, R. Ergun, R. W. Hartel and P. T. Spicer, *Soft Matter*, 2011, **7**, 7710.
- 17 M. Caggioni, J. Lenis, A. V. Bayles, E. M. Furst and P. T. Spicer, *Langmuir*, 2015, **31**, 8558–8565.
- 18 Y. Zhang and Y. Zhai, *Adv. Induction Microw. Heat. Miner. Org. Mater.*, InTech, 2011, pp. 483–500.
- 19 C. S. S. R. Kumar and F. Mohammad, *Adv. Drug Deliv. Rev.*, 2011, **63**, 789–808.
- 20 A. B. Pawar, M. Caggioni, R. W. Hartel and P. T. Spicer, *Faraday Discuss.*, 2012, **158**, 341–350.
- 21 T. A. Prileszky and E. M. Furst, *Chem. Mater.*, 2016, **28**, 3734–3740.
- 22 T. A. Prileszky, B. A. Ogunnaike and E. M. Furst, *AIChE J.*, 2016, **62**, 2923–2928.
- 23 M. H. Rashid, *Power Electronics Handbook*, Elsevier Inc., Oxford, 3rd edn, 2011.
- 24 J. H. E. Promislow and A. P. Gast, *Phys. Rev. E*, 1997, **56**, 642–651.
- 25 A. V. Bayles, T. A. Prileszky, P. T. Spicer and E. M. Furst, *Langmuir*, 2018, **34**, 4116–4121.
- 26 C. Hao, Z. Xie, T. J. Atherton and P. T. Spicer, *Langmuir*, 2018, **34**, 12379–12386.
- 27 F. Perrin, *J. Phys. le Radium*, 1934, **5**, 497–511.
- 28 B. Fischer, B. Huke, M. Lücke and R. Hempelmann, *J. Magn. Magn. Mater.*, 2005, **289**, 74–77.
- 29 W. F. Brown, *Phys. Rev.*, 1963, **130**, 1677–1686.



40x20mm (300 x 300 DPI)